https://doi.org/10.20575/00000027
Polar Data Journal, Vol. 5, 60–68, April 2021

Sea-ice motion and oceanographic data from the Beaufort Sea to the Chukchi Borderland in March–December 2020

Satoshi Kimura[1]*, Takashi Kikuchi[1], Amane Fujiwara[1], Andrew Mahoney[2], Hajo Eicken[3] and Theodore Goda[4]

[1] Japan Agency for Marine-Earth Science and Technology, 2-15 Natsushima-cho, Yokosuka, Kanagawa 237-0061.

[2] Geophysical Institute, University of Alaska Fairbanks, 2156 Koyukuk Drive, AK 99775.

[3] International Arctic Research Center, University of Alaska Fairbanks, 1810 Salcha Street 102 Signers' Hall, AK 99775-7480.

[4] Undersea Warfighting Development Center Arctic Submarine Laboratory, 140 Sylvester Rd. San Diego, CA 92106-3521.

*Corresponding author: Satoshi Kimura (skimura@jamstec.go.jp)

(Received January 13, 2021; Accepted March 3, 2021)

Abstract: Sea-ice reduction is one of the most visible indicators of the Arctic warming. While there are many observations in the interior of the Arctic Ocean, oceanographic and sea-ice trajectory observations near the edge of sea-ice extent are rare. Here, we present oceanographic observations beneath sea ice obtained by an ice-tethered buoy and surrounding sea-ice motions obtained from 9 GPS buoys in the late ice-growth and sea-ice melt season along trajectories from the Beaufort Sea to the Chukchi Borderland in the Pacific sector of the Arctic Ocean.

1. Background & Summary

The drift speed of Arctic sea ice has increased in the last few decades, while the wind forcing has remained relatively stable (Rampal, Weiss, and Marsan 2009)[1]. This indicates a reduction in the regional scale strength of sea ice, such as through loss of thicker, older ice (Kwok 2006)[2], making sea ice more susceptible to deformation and breakup events. The long-term decrease in sea-ice area in the Arctic Ocean is dominated by two regional trends: i) wintertime sea-ice reduction in the Barents Sea (Atlantic sector), and ii) summertime sea-ice reduction over the Siberian Shelves and the Canadian

Basin (Pacific sector). Winter sea-ice reduction in the Barents Sea has been well documented and investigated as a part of the warming of the Atlantic water inflow through the Fram Strait and Barents Sea Opening (Årthun *et al.* 2012[3]; Onarheim *et al.* 2015[4]). In the Pacific sector, there are two possible factors involved in the reduction of sea ice: 1) warming in the Canada Basin (Timmermans *et al.* 2014)[5] due to an increase in the heat flux from the Pacific inflow (Woodgate *et al.* 2012)[6] and 2) ice-albedo feedback process (e.g., Perovich *et al.* 2007[7]; Kashiwase *et al.* 2017[8]). However, the prediction of sea ice changes in seasonal and longer time scales remains to be difficult. The summer sea-ice reduction in the Pacific Arctic sector remains to be a topic of active research, especially to quantify links between sea ice dynamics and oceanographic process.

Much of what we know about sea-ice deformation has been derived from the analysis of GPS buoys on sea ice (e.g., Marsan *et al.* 2004[9]; Itkin *et al.* 2017[10]; Hutchings *et al.* 2011[11]). These GPS buoys are separated by more than ~10 km with a sampling frequency of every 2-3 hours. The deformation characteristics derived from these GPS buoys have been compared to sea-ice models (Bouillon and Rampal 2015)[12]. As computational power and hence model resolution increases, the spatial and temporal scales sampled by GPS buoys will not be adequate for model development and evaluation. Some sea-ice models are beginning to simulate scales of motions less than 10 km (e.g. Mohammadi-Aragh, Losch, and Goessling 2020[13]; Hutter and Losch 2020[14]; Ringeisen *et al.* 2019[15]). There is a need to better understand the deformation at smaller scales (~100 m) in relation to ~10 km-scale motion. Here, we present GPS data of the movement of sea-ice floes ranging from scales of ~100 m up to ~100 km, obtained alongside data on oceanographic conditions using an ice-tethered Warming and Irradiance Measuring (WARM) buoy.

2. Observation Site

A total of 9 GPS buoys and one WARM buoy (Table 1) were deployed approximately 90 km northeast of Prudhoe Bay, Alaska on drifting sea ice centered around Camp Seadragon during the U.S. Navy's ICEX 2020 exercise in March 2020. Our observations extend from the Beaufort Sea to the Chukchi Borderland in March–October 2020 (Figure 1).

3. Methods

Buoy Design

On March 12, five "Universal Tracker" (UT) GPS buoys (JAM-UT-0001–JAM-UT-0005) and four "Ice Tracker" (IT) GPS buoys (JAM-IT-0001–JAM-IT-0004) were placed in two concentric clusters, centered on Camp Seadragon. The inner cluster was approximately 500 m in radius and consisted of the 5 UT buoys. The outer cluster was approximately 10 km in radius and was comprised of the 4 IT buoys. The ice-tethered Warming and Irradiance Measuring (WARM) buoy (JAM-WB-0003) was deployed at the center of these clusters on March 20th, 2020 (Figure 2). The Ice Tracker, Universal Tracker, and WARM buoy are off-the-shelf commercial products, engineered by Pacific Gyre Inc. (https://www.pacificgyre.com). The accuracy of the GPSs is the GPS standard of 3.5 meters. The WARM buoy consists of one temperature sensor 3 m below the ice and a CTD (SBE 37-IM MicroCAT) 10 m below (Figure 3). The temperature and CTD sensors were calibrated from the manufacture, Pacific Gyre Inc. and Sea-Bird Scientific, respectively. The manufacture stated initial accuracy of the SBE 37-IM MicroCAT is ±0.002 ℃. The WARM buoy was tested before the deployment in the open ocean. All the variables are sampled every 30 minutes.

4. Data Overview and Evaluation

The distance between JAM-WB-0003 and other buoys was nearly steady until mid-June (Figure 4a). As the buoys approached Barrow Canyon in mid-June, distances start to diverge, with sea ice exposed to warmer and fresher water (Figure 4b, c). Data from the ICEX 2020 array were compared to data from the Ice Tethered Platform (ITP) program led by Wood Hole Oceanographic Institution, with data available at the ITP website (https://www.whoi.edu/website/itp/overview). The nearest ITP, ITP #114, profiles every 2–4 hours with a vertical resolution of ~1 m. The comparison was made by extracting the profile data between 9 dbar and 14 dbar, which corresponds to the depth of the JAM-WB-0003 sensor. The sampling rate of the ITP is not as high as the sensors in JAM-WB-0003; however, the profiler data has enough temporal resolution to detect fluctuations shorter than a day. The ITP #114 showed trends in temperature and salinity similar to that of JAM-WB-0003 (Figure 4b, c), even though ITP #114 was 500 km away from JAM-WB-0003 (Figure 4a). Although the long-term trend in temperature and salinity records are similar to the ITP measurements, the buoy records contain short time-scale fluctuations (e.g., a rapid salinity increase in Aug 1st). The magnitude of the salinity increase is at most 2.5 PSU in 30 minutes. The magnitude of salinity fluctuation similar to this has been reported in this area (e.g., Kimura *et al.* 2019)[16]. As the ice thins during the summer, the buoy sinks to the ocean, which results in increasing the pressure (Figure 4d). All the GPS buoys were separated by ~100 km from JAM-WB-0003 by the beginning of September. The increase in pressure fluctuation in fall (September–November) indicates that the buoy is in the open ocean (Figure 4d). All the GPS buoys had ceased data transmission by the beginning of October (Table 1).

5. Data Records

The raw data have been organized into the 10 NetCDF (Network Common Data Form) files with filenames corresponding to the device names. The device names and record lengths are indicated in Table 1. Each file contains latitude and longitude from the GPS with variable names, "Latitude" and "Longitude". The sampling time is stored as variable names, "Year", "Month", "Day", "Hour", "Minute", and "Second". In addition to these variables, the data file from the ice-tethered buoy (DATA_JAM-WB-0003.nc) contains 2 temperature, salinity, and pressure records. The variable names and the depth of the record are shown in Figure 3.

NetCDF is a machine-independent data formats that supports the creation, access, and sharing of array-oriented scientific data through various programming interfaces. The details of the NetCDF format are given at the web manual page (https://www.unidata.ucar.edu/software/netcdf/).

7. Figures

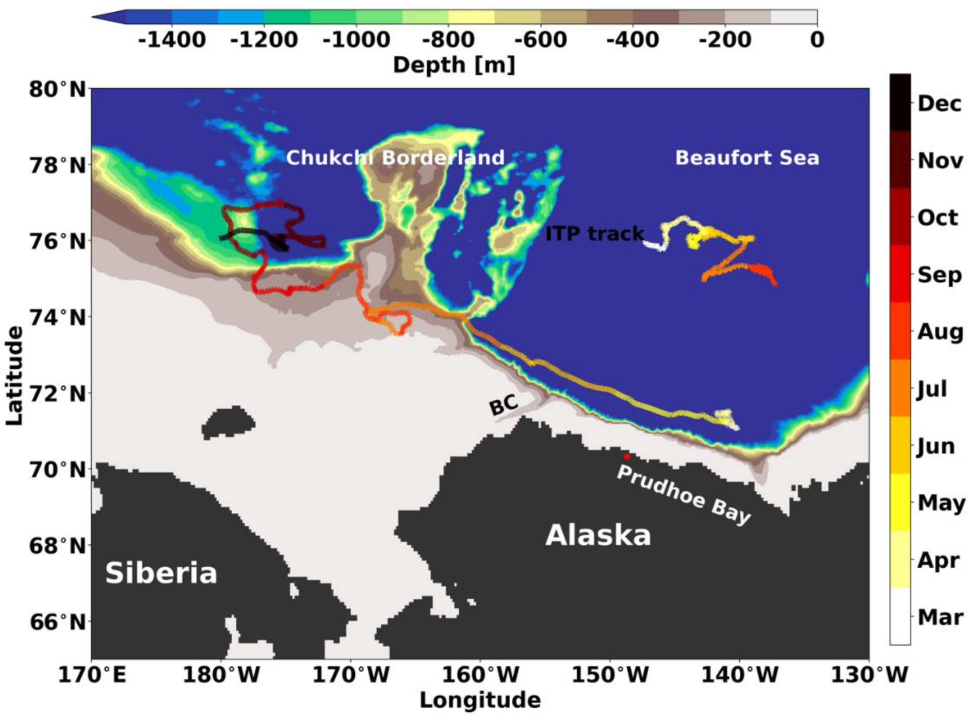

Figure 1. Bathymetry of the Beaufort Sea to the Chukchi Borderland and the JAM-WB-0003 buoy and ITP #114 tracks. The location of Barrow Canyon is indicated by BC.

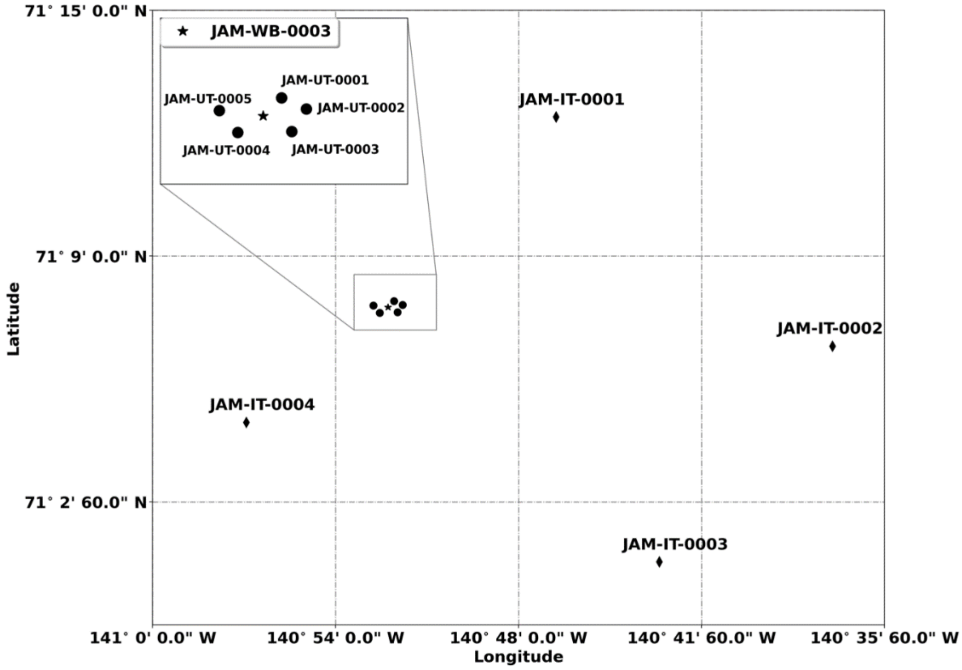

Figure 2. Initial positions of GPS buoys and the ice-tethered buoy on March 20th, 2020 Latitude and longitude are displayed in sexagesimal degree.

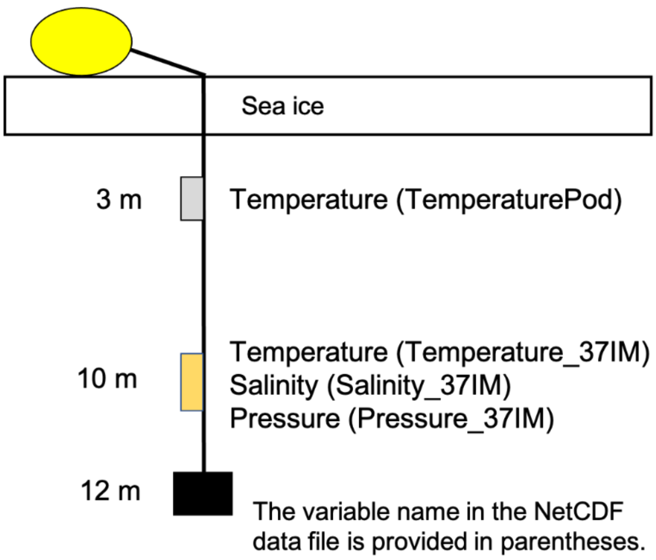

Figure 3. Design of ice-tethered buoy JAM-WB-0003 and the variable names in the NetCDF data file. The temperature pod is placed approximately 3 m beneath the ice, indicated by the gray rectangle. The CTD (SBE 37-IM MicroCAT) is placed 10 m below, indicated by the dark yellow rectangle. The black rectangle indicates the bottom weight at 12 m. The parentheses correspond to the variable names in the NetCDF data file.

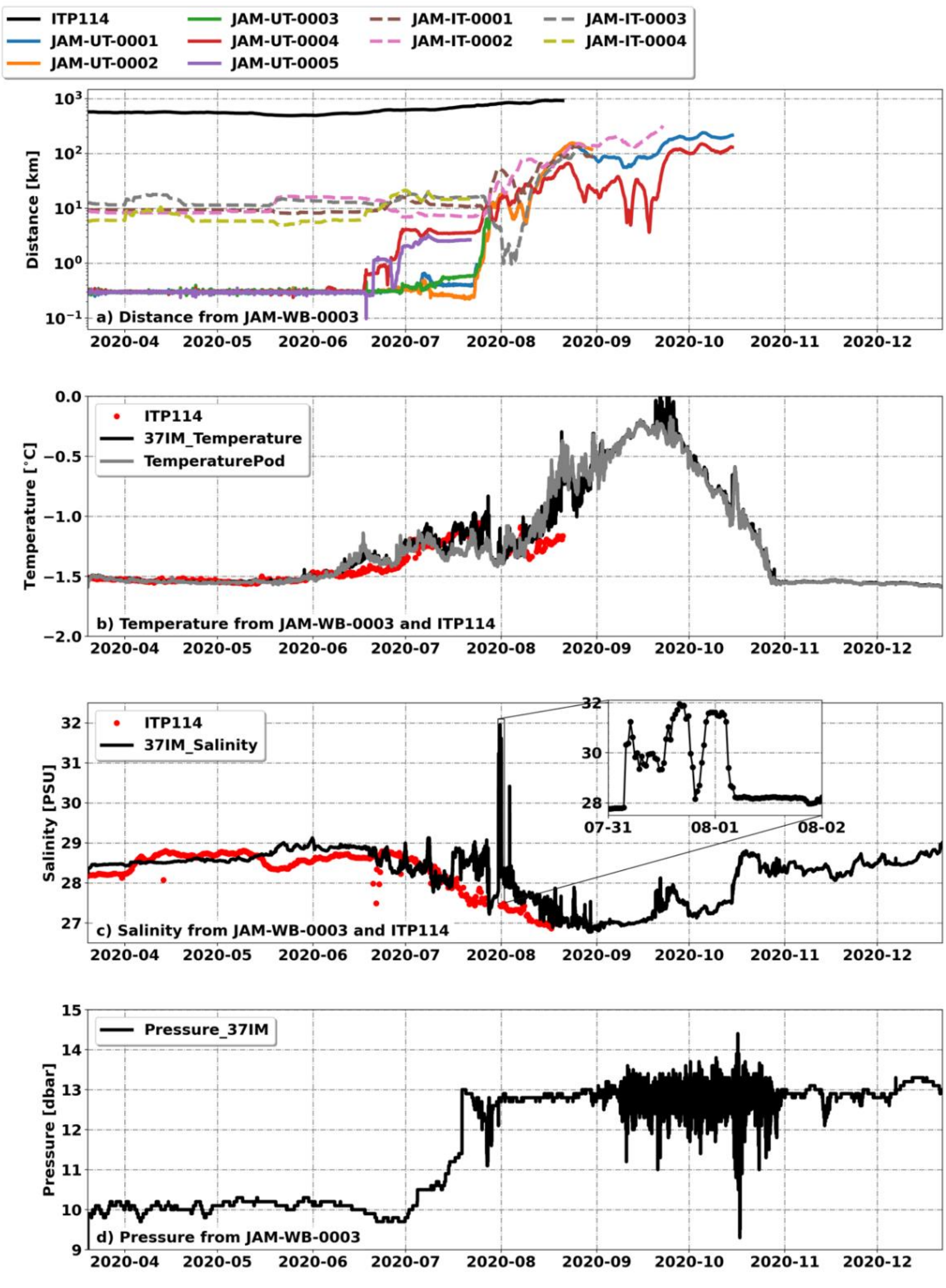

Figure 4. GPS, temperature, salinity, and pressure data during the operational lifetime of buoys and ITP 114: a) distance between JAM-WB-0003 and other buoys with respect to time. b) ITP114 temperature and the JAM-WB-0003 temperature. c) ITP114 salinity and the JAM-WB-0003 salinity. d) pressure record from JAM-WB-0003.

8. Table

Table 1. List of buoys deployed at the Ice Camp Seadragon during ICEX 2020.

Device name	Type	Deployment Date	Deployment Location (latitude, longtitude)	Total Duration (Days)	IMEI
JAM-WB-0003	Ice-tethered buoy	March 20, 2020	71º7'45.33"N, 140º52'16.62"W	277	300234067939910
JAM-UT-0001	GPS, Universal Tracker	March 12, 2020	71º10'37.37"N, 142º24'31.28"W	216	300534060210320
JAM-UT-0002	GPS, Universal Tracker	March 12, 2020	71º10'37.35"N, 142º24'31.12"W	171	300534060216300
JAM-UT-0003	GPS, Universal Tracker	March 12, 2020	71º10'37.29"N, 142º24'31.13"W	138	300534060315140
JAM-UT-0004	GPS, Universal Tracker	March 12, 2020	71º10'37.35"N, 142º24'31.26"W	216	300534060316760
JAM-UT-0005	GPS, Universal Tracker	March 12, 2020	71º10'37.33"N, 142º24'31.32"W	131	300534060318120
JAM-IT-0001	GPS, Ice Tracker	March 12, 2020	71º10'37.58"N, 142º24'31.39"W	172	300534060211310
JAM-IT-0002	GPS, Ice Tracker	March 12, 2020	71º10'37.54"N, 142º24'31.41"W	194	300534060211320
JAM-IT-0003	GPS, Ice Tracker	March 12, 2020	71º10'37.57"N, 142º24'31.44"W	165	300534060312160
JAM-IT-0004	GPS, Ice Tracker	March 12, 2020	71º10'37.60"N, 142º24'31.38"W	133	300534060312770

References

1. Rampal, P., Weiss, J. and Marsan, D. Positive trend in the mean speed and deformation rate of Arctic sea ice, 1979–2007. Journal of Geophysical Research: Oceans. 2009, 114 (C5). https://doi.org/10.1029/2008JC005066.
2. Kwok, R. Contrasts in sea ice deformation and production in the Arctic seasonal and perennial ice zones. Journal of Geophysical Research: Oceans. 2006, 111 (C11). https://doi.org/10.1029/2005JC003246.
3. Årthun, M., Eldevik, T., Smedsrud, L. H., Skagseth, Ø. and Ingvaldsen, R. B. Quantifying the Influence of Atlantic Heat on Barents Sea Ice Variability and Retreat, Journal of Climate. 2012, 25 (13), p. 4736–4743. https://doi.org/10.1175/JCLI-D-11-00466.1.
4. Onarheim, I. H., Eldevik, T., Årthun, M., Ingvaldsen, R. B. and Smedsrud, L.H. Skillful prediction of Barents Sea ice cover. Geophysical Research Letters. 2015, 42 (13), p. 5364–5371. https://doi.org/10.1002/2015GL064359.
5. Timmermans, M.-L., Proshutinsky, A., Golubeva, E., Jackson, J. M., Krishfield, R., McCall, M., Platov, J. *et al.* Mechanisms of Pacific Summer Water variability in the Arctic's Central Canada Basin."

Journal of Geophysical Research: Oceans. 2014, 119 (11), p. 7523–7548. https://doi.org/10.1002/2014JC010273.

6. Woodgate, R. A., Weingartner, T. J. and Lindsay, R. Observed increases in Bering Strait oceanic fluxes from the Pacific to the Arctic from 2001 to 2011 and their impacts on the Arctic Ocean water column. Geophysical Research Letters. 2012, 39 (24). https://doi.org/10.1029/2012GL054092.
7. Perovich, D. K., Light, B., Eicken, H., Jones, K. F., Runciman, K. and Nghiem, S. V. Increasing solar heating of the Arctic Ocean and adjacent seas, 1979–2005: Attribution and role in the ice-albedo feedback. Geophysical Research Letters. 2007, 34 (19). https://doi.org/10.1029/2007GL031480.
8. Kashiwase, H., Ohshima, K. I., Nihashi, S. and Eicken, H. Evidence for Ice-Ocean Albedo Feedback in the Arctic Ocean Shifting to a Seasonal Ice Zone. Scientific Reports. 2017, 7 (1), 8170. https://doi.org/10.1038/s41598-017-08467-z.
9. Marsan, D., Stern, H., Lindsay, R. and Weiss, J. Scale Dependence and Localization of the Deformation of Arctic Sea Ice. Physical Review Letters. 2004, 93 (17), 178501. https://doi.org/10.1103/PhysRevLett.93.178501.
10. Itkin, P., Spreen, G., Cheng, B., Doble, M., Girard-Ardhuin, F., Haapala, J., Hughes, N., Kaleschke, L., Nicolaus, M. and Wilkinson, J. Thin ice and storms: Sea ice deformation from buoy arrays deployed during N-ICE2015. Journal of Geophysical Research: Oceans. 2017, 122 (6), p. 4661–4674. https://doi.org/10.1002/2016JC012403.
11. Hutchings, J. K., Roberts, A., Geiger, C. A. and Richter-Menge, J. Spatial and temporal characterization of sea-ice deformation. Annals of Glaciology. 2011, 52 (57), p. 360–368. https://doi.org/10.3189/172756411795931769.
12. Bouillon, S. and Rampal, P. Presentation of the dynamical core of neXtSIM, a new sea ice model. Ocean Modelling. 2015, 91, p. 23–37. https://doi.org/10.1016/j.ocemod.2015.04.005.
13. Mohammadi-Aragh, M., Losch, M. and Goessling, H. F. Comparing Arctic Sea Ice Model Simulations to Satellite Observations by Multiscale Directional Analysis of Linear Kinematic Features. Monthly Weather Review. 2020, 148 (8), p. 3287–3303. https://doi.org/10.1175/MWR-D-19-0359.1.
14. Hutter, N., and Losch, M. Feature-based comparison of sea ice deformation in lead-permitting sea ice simulations. The Cryosphere. 2020, 14 (1), p. 93–113. https://doi.org/10.5194/tc-14-93-2020.
15. Ringeisen, D., Losch, M., Tremblay, L. B. and Hutter, N. Simulating intersection angles between conjugate faults in sea ice with different viscous–plastic rheologies. The Cryosphere. 2019, 13 (4), p. 1167–1186. https://doi.org/10.5194/tc-13-1167-2019.
16. Kimura, S., Onodera, J., Itoh, M., Kikuchi, T., Nishino, S., Kawaguchi, Y., Watanabe, E. and Harada, N. The Warming of the Chukchi Slope Through the Barrow Canyon Outflow in the 2016–2017 Winter. Journal of Geophysical Research: Oceans. 2019, 124 (11), p. 7437–7456. https://doi.org/10.1029/2019JC015093.

Data Citation

Kimura, S., Kikuchi, T., Fujiwara, A., Mahoney, A., Eicken, H. and Goda, T. Sea-ice motion and oceanographic data from the Beaufort Sea to the Chukchi Borderland in March-December, 2020. 1.00, Japan, Arctic Data archive System (ADS), 2021. https://doi.org/10.17592/001.2021012801.